GeoScienceWorld
Lithosphere
Volume 2022, Article ID 7562666, 14 pages
https://doi.org/10.2113/2022/7562666

Lithosphere

*Research Article*

# Climate-Driven Changes in High-Intensity Wildfire on Orbital Timescales in Eurasia since 320 ka

**Tianze Cheng**,[1] **Jianjun Zou**,[2,3] **Xuefa Shi**,[2,3] **Sergey Gorbarenko**,[4] **Yuriy Vasilenko**,[4] **Alexandr Bosin**,[4] **Yanguang Liu**,[2,3] **and Bing Chen**[1,3]

[1]*Environment Research Institute, Shandong University, Qingdao 266237, China*
[2]*Key Laboratory of Marine Geology and Metallogeny, First Institute of Oceanography, Ministry of Natural Resources, Qingdao 266061, China*
[3]*Pilot National Laboratory for Marine Science and Technology (Qingdao), Qingdao 266061, China*
[4]*V.I. Il'ichev Pacific Oceanological Institute, Far East Branch of the Russian Academy of Sciences, Vladivostok, Russia*

Correspondence should be addressed to Jianjun Zou; zoujianjun@fio.org.cn, Xuefa Shi; xfshi@fio.org.cn, and Bing Chen; bingchen@sdu.edu.cn

Received 11 January 2022; Accepted 6 June 2022; Published 16 June 2022

Academic Editor: Feng Cheng



Wildfire is an integral part of the Earth's climate system and plays an important role in shaping terrestrial ecosystems and biodiversity, atmospheric chemistry, regional climate, and the carbon cycle in the Earth's history. However, the lack of high-resolution records of long wildfires limits our understanding of the natural variability, long-term trends of wildfire activity, and the reasons behind the changes in wildfire on orbital timescales. Here, a 320 ka long high-resolution wildfire record from the subarctic North Pacific is reconstructed with black carbon (BC), including its two subtypes char and soot. A 7-day-long back trajectory simulation analysis reveals the higher frequency of trajectories comes from Siberia. Our data show that continuous incidence of wildfire on a continental scale over the last 320 ka was higher during glacial periods than during the interglacial periods. The increase in wildfire frequency during glacial periods is ascribed to less precipitation. Contrasting patterns of wildfire incidence between marine isotope stages 2 and 6 may be ascribed to different fuel availability, which is related to contrasting configurations of the Northern Hemisphere ice sheet between glacial periods. A significant periodicity of 23 ka of our wildfire record suggests the precession of the Earth's orbit pace wildfire development. The tight coupling of intensified wildfire and enhanced nutrient utilization efficiency suggests a nontrivial role of fire in the climate system.

## 1. Introduction

As one of the key players in the climate system [1, 2], wildfire significantly impacts global climate and environmental change by releasing heat, gases, and substances, changing surface albedo, and affecting radiative forcing components [1]. For example, a large amount of carbon dioxide ($CO_2$), methane ($CH_4$), black carbon (BC), and other greenhouse gases emitted into the atmosphere during the combustion of biomass could contribute to global warming [3, 4]. Wildfire also can reshape the development, growth, and succession of terrestrial vegetation and its community structure and thus reshaping the landscapes [1, 5]. Many researchers have attempted to understand the occurrence, variations, and driven mechanisms of wildfire and the relationships between wildfire and climate and vegetation on various temporal and spatial scales [6, 7]. However, the patterns and driving forces of fire activity in the past remain elusive. Long-term records of wildfire frequency, integrated in a large continental area over glacial-interglacial cycles, can provide insight into the natural variability and long-term trends of wildfire [8]. Therefore, the long-term proxy record of biomass burning is very invaluable. However, the knowledge of wildfire over glacial cycles in the Eurasia inland region remains elusive today.

Wildfires range from slow smoldering peat fires to low-intensity ground fires and intense burning canopy fires. The main factors controlling wildfire types include fuel availability, vegetation types, prevailing climate, and weather conditions [2, 9]. Weather patterns determine the flammability of fuel over short timescales, while on a long timescale, the temporal and spatial patterns of wildfire frequency and scope are vulnerable to seasonal climate change (wet or dry), which will affect the availability of fuel and vegetation type [4, 10]. Previous studies have shown that high-intensity wildfires on the Chinese Loess Plateau during the Holocene, in which the East Asian summer monsoon climate dominates, are caused by low water content of fuel due to seasonal precipitation [10–12]. Drought promotes wildfire by reducing fuel moisture. A statistical analysis of fire data around the world also indicates that there is more rainfall and lower combustion efficiency; thus, wildfire frequency is lower under humid climate conditions [13, 14]. This has been validated by wildfire records in Africa [15, 16]. In the savannah of Africa, the annual rainfall of more than 800 mm tends to hinder the fire, mainly because the dry season is not long enough to make grass fuel catch fire. The long dry seasons and the relatively rapid accumulation of fuel create conditions for frequent fires.

Various proxies have been used to reconstruct the history of wildfire, including charcoal, black carbon (BC), tree fire scars, and polycyclic aromatic hydrocarbons (PAHs) [12, 17]. Charcoal and BC produced directly by fire combustion can be widely preserved in loess, lakes, and marine sediments due to their decay-resistant chemical properties and inertness. BC does not refer to a single well-defined compound because carbonaceous aerosols are emitted as a continuum of compounds with different physical and chemical properties. Moreover, they have been widely used as excellent archives to record the information of ancient wildfires [4, 6, 18–20]. The potential deviation of some opaque minerals makes it easy to overestimate the wildfire regimes based on charcoal [21]. By contrast, BC covers a more complete spectrum of fire residues [14], which are completely generated from the incomplete combustion of terrestrial vegetation. Several studies have shown that the BC may be a more robust proxy of wildfires than charcoal, especially in regional or hemispheric wildfires [12, 18, 20, 22]. The BC in sediments from the geological past has also been used to check the long-term variations in fire occurrence [12, 23]. Meanwhile, char and soot [3, 23] have been proven to be able to distinguish the fire types more accurately, such as smoldering and flaming [3, 13, 24]. Char and soot, for example, typically have different particle sizes [24, 25], which can lead to different transport patterns and distances [26]. Char usually reflects a local low-intensity wildfire. In contrast, the size of soot is less than 1 $\mu$m and it is formed at higher temperatures, which reflects the biomass combustion in a larger area [22].

The ocean is considered as the final sink for burning residues, and BC has been widely identified in sediments around the global ocean [9, 25, 27, 28]. Compared with terrestrial archives, the BC in deep-sea sediments, especially from the open ocean far away from the biomass combustion sources, is mainly transported to the study site by the wind. To date, there are still few long-term records of wildfire from sediments in the subarctic Pacific.

In this study, we investigate the wildfire history over the last 320 ka on the basis of high-resolution measurements on BC in sediments of core LV76-18 retrieved from the Detroit Seamount in the subarctic Pacific. The long-term trends of wildfire frequency and the reasons behind the changes in wildfire are revealed. Our results provide new insights into the relationship between wildfire and climate.

## 2. Materials and Methods

*2.1. Study Site and Oceanographic Settings.* As shown in Figure 1, an 810 cm long sediment core LV76-18 was taken from the western flank of the Detroit Seamount in the Northwest Subarctic Pacific (49.05°N, 168.55°E, water depth 2863 m) during the China-Russia joint expedition in the Northwestern Pacific with R/V Lavrentyev from July to August 2016. The study core is located directly downwind of the northern westerly wind. The Siberian inland has experienced large changes in fire incidence in response both to large-scale global climate changes and the impact of recent anthropogenic activities.

A 7-day-long back trajectory simulation analysis calculated with the Hybrid Single-Particle Lagrangian Integrated Trajectory Model (HYSPLIT) starting from the sampling site indicates four main pathways of atmospheric trajectories for the transmission of wildfire residues to the sampling sites, with three routes coming from the Siberia and accounting for about 90% of the total number of trajectories. Other contributors to the air masses are North America. The investigations of sediment provenance in the study area show that the fine-grained terrigenous sediments deposited in the subarctic North Pacific are mainly derived from the dust in the Asian interior delivered by the northern westerly [30]. When big fires occur broke out in the interior of Siberia, it was thought that the burning residues from land must be taken to the study areas thousands of kilometers away from the burning area. Thus, the wildfire records from core LV76-18 in the subarctic North Pacific mainly reflect the history of wildfire in the Siberian interior.

In the terrestrial environment, the signals of regional and local fires may overlap, and the interpretation of wildfire records can be more complicated by local factors. However, in the subarctic Pacific far away from land, it is more reliable to provide a high-resolution and long-term continuous record of average frequency of wildfires on the continental scale.

The sediment core was measured with an X-ray fluorescence core scanning (XRF-CS) housed at the First Institute of Oceanography, Ministry of Natural Resources. XRF-CS data were measured at an interval of 1 cm along with the core in three runs with 10 kV, 30 kV, and 50 kV. A high-resolution XRF scanner-based Ba/Fe ratio was chosen to tune to the LR04 $\delta^{18}$O stack [31].

The age model for core LV76-18 was determined using a combination of one radiocarbon date [32] and tie points by correlating the Ba/Fe ratio with LR04 $\delta^{18}$O stack [31]

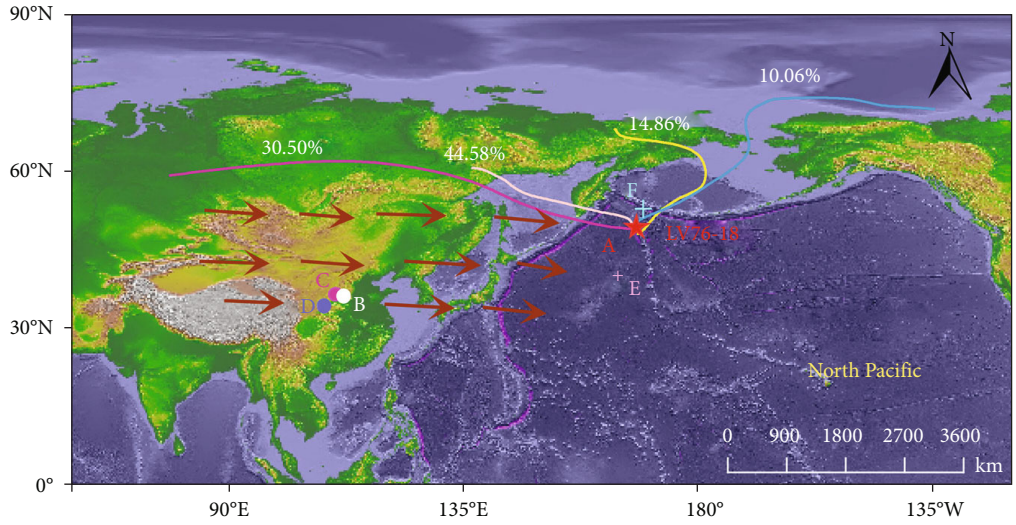


Figure 1: A 7-day air mass backward-trajectory analysis from study site LV76-18 (red star). The base map is generated from the MeteoInfo software [29] (free version 2.3.4). A total of 744 backward trajectories were obtained from the HYSPLIT model, and four main trajectories were simulated according to the Euler clustering method. Percentage represents the proportion that each cluster trajectory contains in the total number of trajectories. The brown arrows indicate the trajectories of westerly. Sites for subsequent comparison include (A) LV76-18 core, (B) Luochuan station, (C) Xifeng station, (D) Baoji station, (E) V21-146 core, and (F) MD01-2416 core.

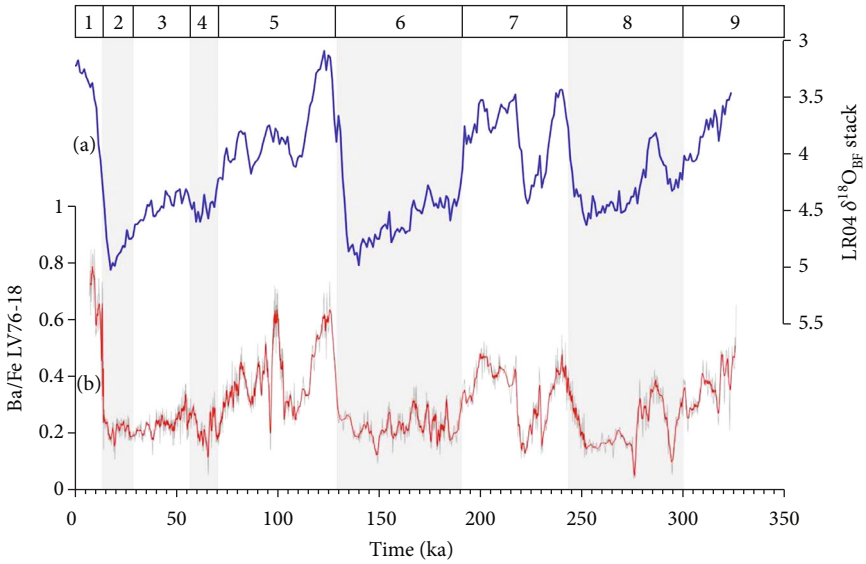


Figure 2: Age model of core LV76-18 in the subarctic Pacific. (a) The solid blue line is the global benthic oxygen isotope stack [31]. (b) The solid red line denotes the 5-point running average of the Ba/Fe ratio, and the light gray curve represents the original Ba/Fe ratio of core LV76-18. The light vertical gray bar denotes glacial periods.

(Figure 2). The age of the sediment core was linearly interpolated between tie points. Linear sedimentation rates (LSR) vary between ~0.7 and ~4.9 cm/ka.

*2.2. Quantification of Sedimentary BC, Char, and Soot.* In recent years, great progress has been made in measuring the BC. Presently, there are several quantitative detection methods for the BC, including chemical thermal oxidation (CTO), thermal-optical reflectance (TOR), and ultraviolet oxidation (UV) [26, 27, 33, 34]. Among these methods, the TOR has the smallest error in measurement between different laboratories, and it has great potential to effectively distinguish char from soot [27]. Consequently, in our study, we adopted the wet-chemical treatment combined with the TOR method to measure the concentration of BC [27]. The TOR method developed by Han et al. has been verified and successfully applied to wildfire reconstructions to detect char and soot components [24, 27, 35].

The sediment subsample was taken at intervals of 1-2 cm in the laboratory and was kept frozen until further

processing. A total of 160 subsamples were selected for BC measurements, and the history of wildfire over the last 320 ka was reconstructed. The samples were pretreated according to the published method [25, 27, 34]. In brief, the samples were freeze-dried and ground into powder. Then, 0.1 g of each sample was weighed and pretreated with HCl and HF to remove carbonates, silicates, and some metals [35]. The remaining residues were then filtered onto a 47 mm precombusted quartz filter. These filters were dried in an oven at 40°C for around six hours for subsequent BC measurements [24, 34].

The samples on filters were analyzed using a Sunset carbon analyzer (Sunset Laboratory, Tigard, USA) and the interagency monitoring of protected visual environment protocol (IMPROVE–H). The instrument adopts a photothermal method, that is to say, it combines pyrolysis and optical methods. We used a pyrolysis program to gradually volatilize the organic carbon (OC) and elemental carbon (EC) components, and then, the segmentation points of OC and EC were corrected by the optical method, which makes the measurements more accurate. According to the protocol, the filter was heated gradually to progressive temperatures of 140°C, 280°C, 480°C, and 580°C in a controlled gas (pure helium environment) and produced four organic carbon (OC) fractions ($OC_1$, $OC_2$, $OC_3$, and $OC_4$). Subsequently, the temperature was further raised to 580°C, 740°C, and 840°C in a 2% oxygen and 98% helium atmosphere, respectively, which produced three corresponding EC fractions ($EC_1$, $EC_2$, and $EC_3$) [24, 25, 27, 35]. The volatile and oxidized carbon gases were oxidized to $CO_2$ and then reduced to $CH_4$, which is detected by a flame ionization detector [34, 36]. In this method, the pyrolytic organic carbon (POC) is produced in the inert gas (He) atmosphere, which could be a part of the OC [24]. The pyrolysis of organic carbon (POC) occurs in 100% He gas. In order to ensure the stability and normal operation of the instrument, a known amount of methane was used to calibrate the instrument. An example of a thermal spectrogram measured by the Sunset carbon analyzer is shown in Figure S1. Based on the protocol, BC can be defined as $EC_1$+$EC_2$+$EC_3$–POC. In addition, char and soot were calculated by $EC_1$–POC and $EC_2$+$EC_3$, respectively [24, 27].

The mass accumulation rate (MAR) ($mg\,cm^{-2}\,ka^{-1}$) of BC, char, and soot were calculated using the following equations [3]:

$$\mathrm{MAR(BC, char, or\ soot)} = C \times \mathrm{BD} \times \mathrm{LSR}, \quad (1)$$

where BD ($g\,cm^{-3}$) is the bulk sediment density, LSR ($cm\,ka^{-1}$) is the linear sedimentation rate, and $C$ ($mg\,g^{-1}$) is the concentration of char, soot, or BC.

*2.3. Quality Assurance and Quality Control.* One of the main factors affecting the accuracy of BC concentration measurement is whether the sample distribution on the filter is uniform or not [25]. Therefore, in order to ensure the reliability of the results, we randomly selected 10% of the filters and repeated the experiment at two different positions on each filter. The relative standard deviation (RSD) measured from the two positions of all samples was less than 5%, and the average was less than 3%. For quality control, standard reference material (marine sediment, NIST SRM-1941b) was also analyzed through the same procedure as for our samples. The average BC concentration of standard samples was $9.97 \pm 0.24\,mg\,g^{-1}$, which is very consistent with the previous studies [27, 34, 35, 37].

## 3. Results

The concentrations and MARs of BC, char, and soot obtained from LV76-18 are shown in Figure 3. BC concentration varies from 0.05 to $1.08\,mg\,g^{-1}$, and the downcore trends of soot and char are consistent with those of BC. Statistics show that there is a strong correlation between BC, char, and soot concentrations (Figure 4), and the correlation coefficient between BC and soot is 0.99, while the correlation coefficient between char and soot is 0.92. The positive correlation indicates that both of them mainly come from the same fire source and are transported to the study site by the same agents.

As the concentrations of BC and its subtypes in sediments are easily affected by many factors, such as the dilution of detrital matter and water content, the MARs can better reflect the real variations in BC input. The records of three indicators showed similar trends, but their corresponding concentrations were not exactly the same. BC-MARs vary between 0.06 and $4.15\,mg\,cm^{-2}\,ka^{-1}$, with an average of $0.97\,mg\,cm^{-2}\,ka^{-1}$. The soot-MARs are much larger than those of char, with the averages of $0.57\,mg\,cm^{-2}\,ka^{-1}$ and $0.4\,mg\,cm^{-2}\,ka^{-1}$, respectively. In general, the increase of MAR values mainly occurred during glacial periods while lower values often occurred during interglacial periods (Figure 3).

The MAR records of three proxies all exhibit prominent orbital-timescale variability (Figure 3). The average MAR values of BC, char, and soot in each marine isotope stage were calculated to quantitatively check the differences between the different time intervals (Figure 5). The data show that the average BC-, char- and soot-MARs during the glacial periods were 1-3 times higher than in interglacial periods (MIS1, 3, 5, 7).

## 4. Discussion

*4.1. Wildfire Activities Recorded in the Record Based on BC.* As mentioned above, for the two subtypes of BC, soot is mainly produced in a high-intensity fire while char is mainly generated in local fire or initial stage of high-intensity fire [3, 23]. Therefore, we qualitatively reconstructed the history of wildfires by the MARs of soot in this study, although the interglacial-glacial patterns of MARs of BC, char, and soot are similar to each other (Figures 3(e)–3(g)). Overall, our data show that the wildfires documented in core LV76-18 persistently occurred over the last 320 ka and the frequency of high-intensity wildfires varied greatly over glacial-interglacial cycles (Figure 3). Figure 3(e) shows that the frequency of wildfire was relatively stable and comparatively low during interglacial periods, while increasing significantly

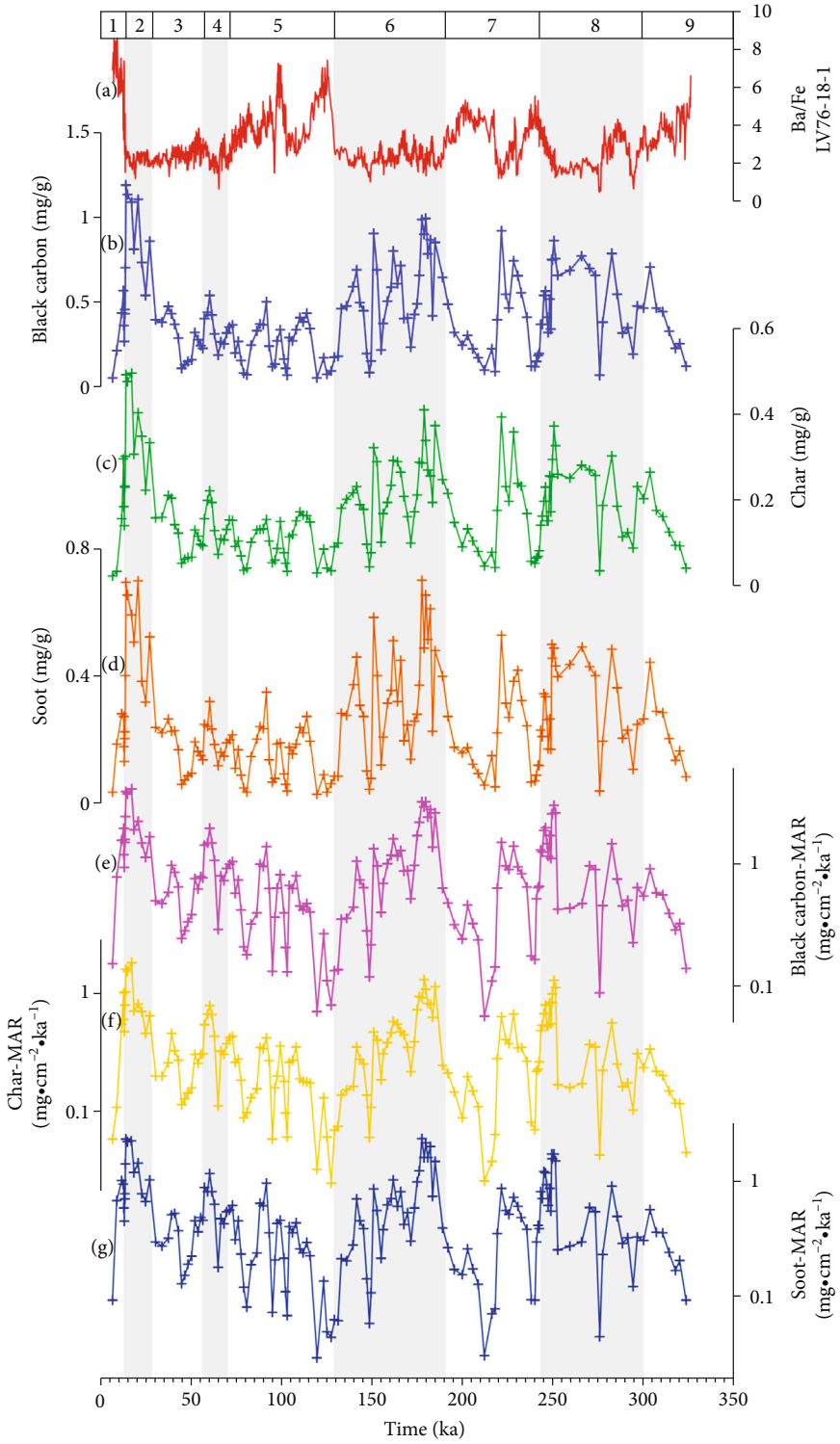


FIGURE 3: Wildfire records reconstructed from black carbon (BC), char, and soot in core LV76-18 over the past 320 ka. (a) LV76-18Ba/Fe ratio; (b) BC concentration; (c) char concentration; (d) soot concentration; (e) BC-MAR; (f) char–MAR; (g) soot-MAR. Gray-shaded bands represent glacial periods. Note the log scale for MAR of BC, char, and soot.

during glacial periods. The result of soot frequency analysis shows that there is a significant period of 23 ka (Figure 6).

Although the frequency of wildfires in glacial periods was higher, there were some variations in different glacial periods. For example, from the early stage to the late stage of MIS6, the frequency of wildfire showed a downward trend (Figure 3(g)). This may be related to the gradual decrease of available fuel loads, but actually related to

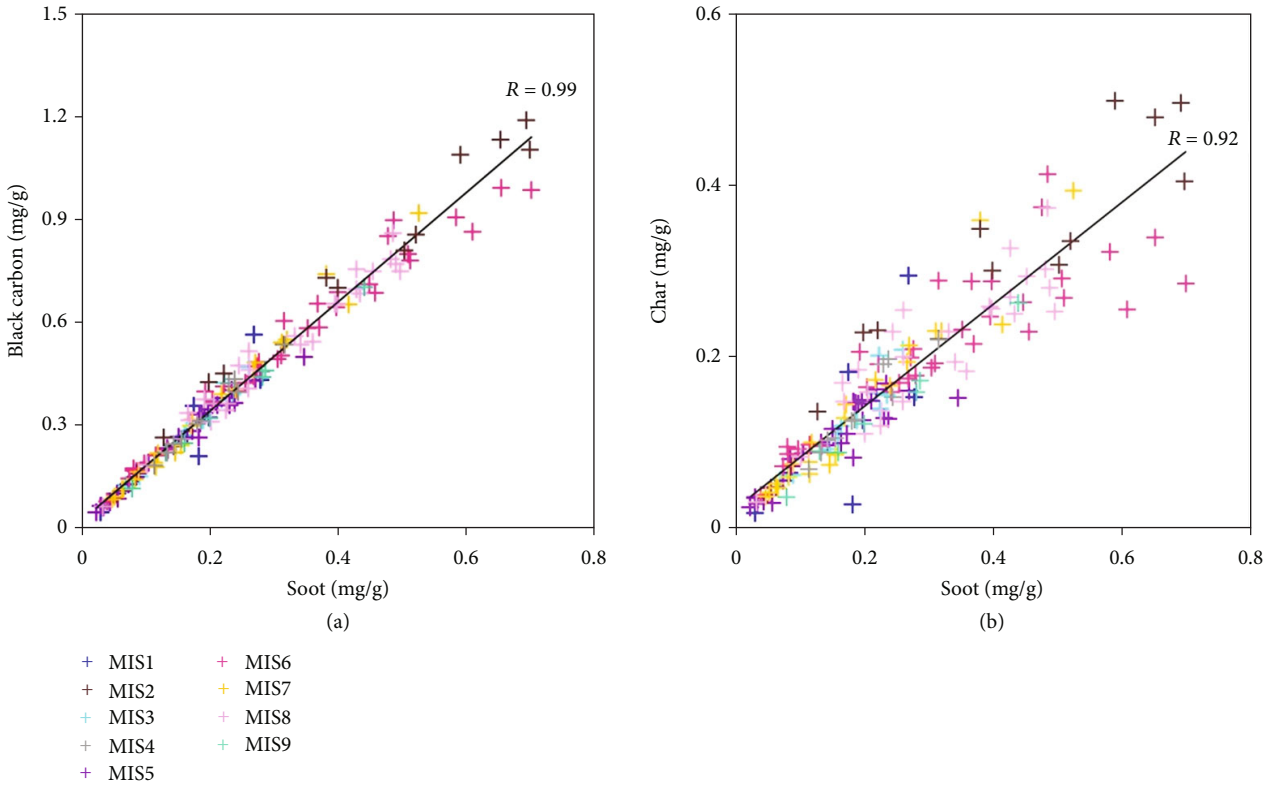


Figure 4: Scatter plots between (a) BC and soot and (b) char and soot of core LV76-18.

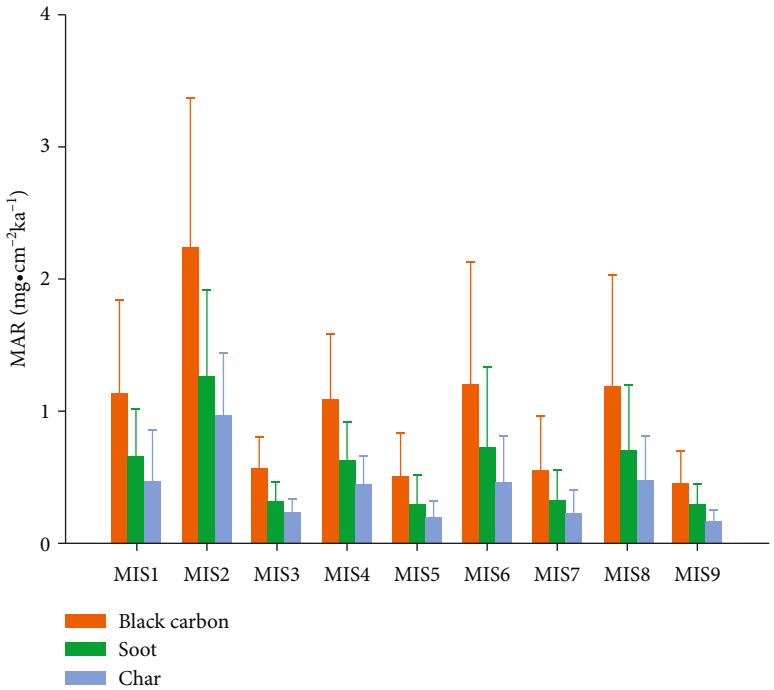


Figure 5: Average mass accumulation rate (MAR) values among BC, soot, and char in different marine isotope stages (MIS) for core LV76-18.

the expansion of ice sheets in the Northern Hemisphere during MIS6. Both observations and simulations showed that during MIS6 the Northern Hemisphere ice sheet coverage is larger than that of the Last Glacial Maximum (LGM), which leads to the reduction of vegetation coverage and fuel loads [38].

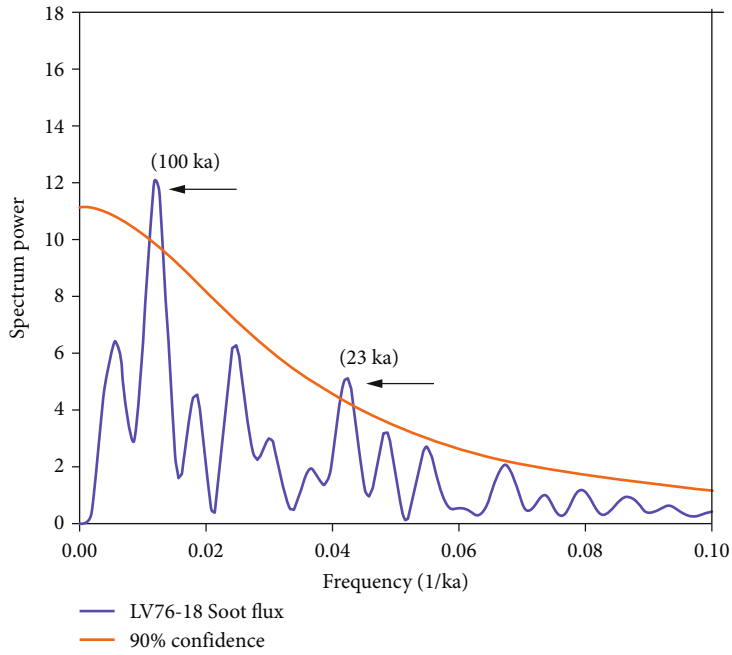


Figure 6: Spectral frequency analysis for soot-MAR of LV76-18 from the subarctic Pacific during the past 320 ka in this study.

On the whole, our wildfire record (Figure 7(b)) is consistent with the Chinese loess (Figure 7(c)). The frequency of wildfire was higher in the glacial periods, and there was an obvious precession cycle in our records. However, it should be clear that there is a significant difference between char and soot in the wildfire record from the Xifeng Loess, that is, there are differences between flaming and smothering on orbital timescales, but in our records, they showed similar trends. This indicates that the char record from Xifeng Loess may be influenced by local wildfires, whereas our wildfire record is more likely to represent regional or hemispheric records. In addition, there are some differences between soot records and loess records during MIS6. The loess records showed that the frequency of wildfire was higher during the late MIS6 and low during the early MIS6, but our record showed a decreasing trend. The differences may be related to the inconsistent regional sources and climate of the wildfire recorded by loess and core LV76-18 in MIS6. An increase in the frequency of glacial wildfires frequency has also been recorded in low-latitude areas, such as cores SHI-9014 in the Banda Sea [7] and MD96-2098 in the Southern African coast [43].

Both these records showed that the frequency of high-intensity wildfires was higher during glacial than in interglacial periods. However, the pattern of high-intensity wildfires differs from other records. According to the charcoal records from lake sediments, the global wildfire records showed that there was a low frequency of wildfire during the LGM and a unidirectional increase in biomass burning during the last deglaciation. The spatial variability of wildfire increased during the interglacial period since 12 ka [44]. During the LGM, lower $CO_2$ concentration and colder, drier climatic conditions prevailed, resulting in a decrease in land biomass and fuel loads [45]. With the retreat of the continental ice sheet in the northern hemisphere, the concentration of $CO_2$ increases, the land vegetation expands, and the fire incidence generally rises [44]. Monosaccharides recorded the prevalence of low-intensity wildfires in sediments of Lake El'gygytgyn (cores PG 1351 and ICDP 5011-1), northeast Siberia, which may be typical features of the Siberian larch forest [46]. Australian charcoal records show that the frequency of wildfire decreased during the glacial periods and increased during the interglacial periods, which is related to the decrease of biomass burning during the cold periods and the increase of biomass burning during the warm periods [21].

An interesting phenomenon is that our wildfire records are in phase with dust from the Loess Plateau (Figure 7(e)) and sediments from the North Pacific Ocean (Figure 7(d)) but are opposite to atmospheric $CO_2$ concentration (Figure 7(h)). This indicates a close interaction between wildfires and orbital-scale climate. As both dust and wildfire plumes contain high levels of nutrients, this will significantly impact on marine productivity, especially in the HNLC (High-Nutrient, Low-Chlorophyll) areas. Based on loess wildfire records, Han et al. speculated that increased wildfire and dust supply during the Asian inland glacial periods contributed to the outburst of surface marine productivity in the Northern Pacific [3]. The Ba/Al ratios in our study (Figure 7(f)) showed that the North Pacific was characterized by low surface productivity during the glacial period, which does not support this speculation. However, we have noticed that the increase in wildfire frequency and dust supply during the glacial periods was closely related to the improved nutrient utilization efficiency, as shown by sedimentary organic matter $\delta^{15}N$ (Figure 7(g)) [41]. This may be because wildfire plumes and dust are rich in micronutrients, such as Fe and P, which help to improve the utilization

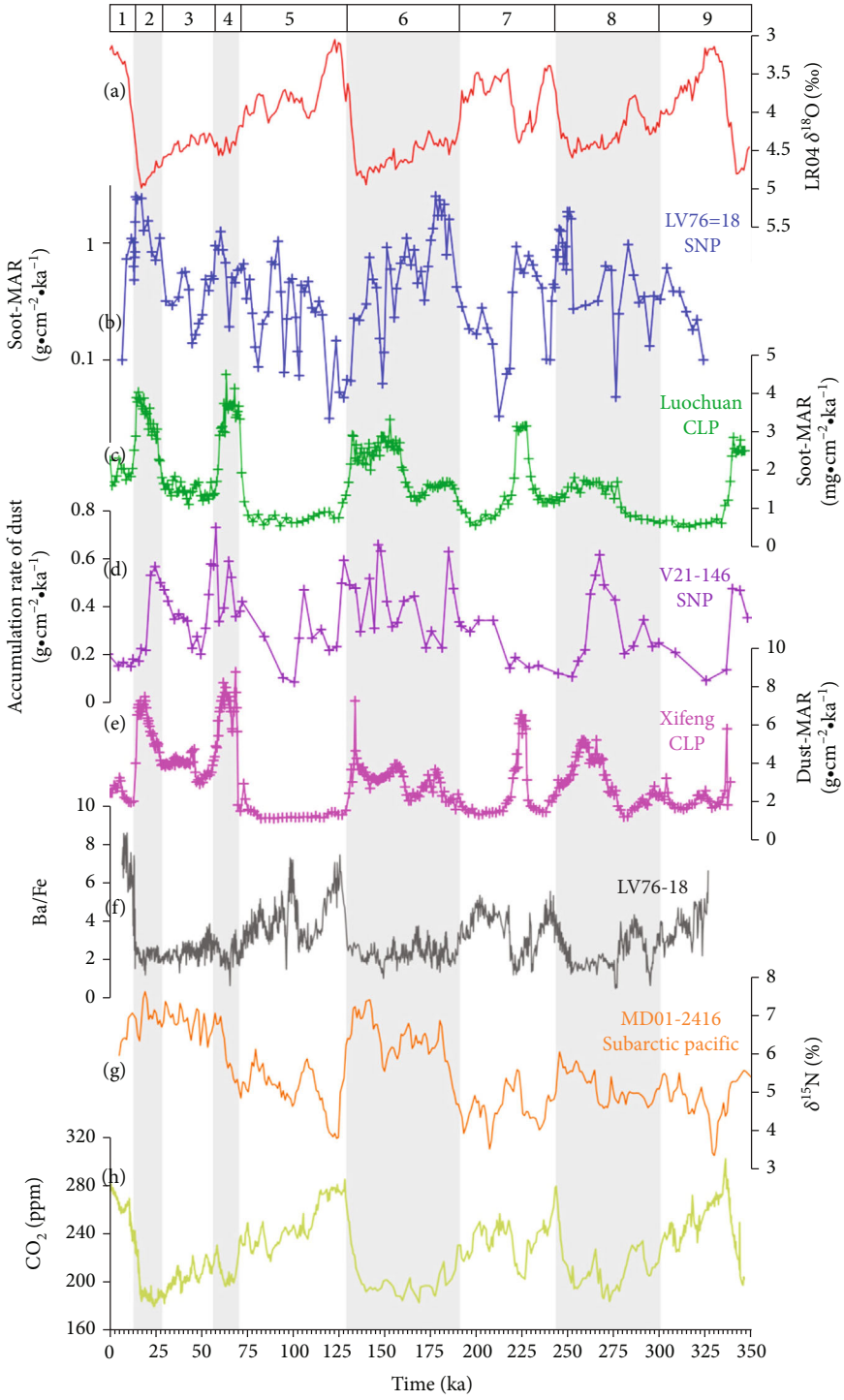


Figure 7: Comparison of the LV76-18 soot record and other wildfire records and global indicators. (a) LR04 $\delta^{18}$O, the global benthic composite oxygen isotope curve [31]; (b) subarctic North Pacific core LV76-18 soot-MARs (this study); (c) Luochuan soot-MARs [3]; (d) V21-146 dust-MARs in the Northwest Pacific [39]; (e) Xifeng dust-MARs [40]; (f) LV76-18 Ba/Fe ratio (this study); (g) MD01-2416 $\delta^{15}$N record in subarctic Pacific [41]; (h) atmospheric $CO_2$ [42].

efficiency of nutrients in the surface ocean. Therefore, we argue that the soluble trace elements from more frequent wildfires during glacial periods, such as Fe and P, have the potential to improve nutrient use efficiency, which is helpful for the removal of $CO_2$ from the atmosphere.

In addition, wildfire also affects the climate by releasing aerosols into the atmosphere and changing the albedo of the land surface. As a by-product of biofuels, BC has strong solar radiation absorption properties and its impact on global warming is second only to $CO_2$ [47]. The reduction

of vegetation coverage caused by high-intensity fires would lead to more bare land, which would increase the albedo of ground surface, especially when the local surface is covered with snow. In fact, the effects of aerosol and surface albedo can sometimes cancel each other out [48].

*4.2. Climate Controls on Orbital-Scale Wildfires.* Our study showed that the frequency of intense Siberian wildfires recorded in core LV76-18 is higher in glacial periods than that in interglacial periods (Figure 8(a)). We suggest that the variations in wildfire frequency on the orbital timescale are restricted by climate, while vegetation cover and fuel loads are regulated by climate. Numerous studies have shown that climate mainly affects global biomass combustion through temperature and precipitation changes. Increased temperature and continued drought can affect fuel flammability and lead to increased wildfire activities on seasonal to centennial time scales [49]. Climate also determines glacier retreat and forest expansion and affects fuel humidity, which will inhibit biomass combustion [50]. Undeniably, different combinations of dry/wet and cold/warm will have more complex impacts on the occurrence of fire activities [51], which may require further studies in combination with other indicators in order to understand the interaction mechanisms between wildfires and climate specifically.

The increase in the frequency of high-intensity wildfire is closely related to decreased precipitation, as evidenced by heavy $\delta^{18}O$ records in the absolutely dated speleothem records of Eastern China and $^{10}Be$ registered in the Xifeng Loess [52–54] (Figures 8(b) and 8(c)). The increase in wildfire activity is inversely correlated with the weak summer monsoon (Figure 8(b)) [53, 55], which brings relatively less precipitation from the tropics, and drought mainly increases the risk of wildfire by reducing fuel moisture. Han et al. attributed the increase in high-intensity wildfire during glacial periods to intensified aridification in the Asian inland at that time. Pechony and Shindell concluded that the global fire regime was strongly driven by precipitation (rather than temperature) during the preindustrial period based on simulations [51]. The high coincidence between our wildfire record with the East Asian summer monsoon (EASM) intensity and precipitation supports the idea that the precipitation (thus available moisture) is the first-order factor in determining the high-intensity wildfire frequency in Siberia. Temperature is another key factor in controlling wildfires. The higher the temperatures, the more wildfires will be caused. Compared with the land surface temperature of the Xifeng Loess (Figure 8(d)), we found that some high-intensity wildfires correspond to the increase in land surface temperature, so temperature can only partially explain the high-intensity fire frequency.

Besides climate, biomass burning is also related to the composition and structure of vegetation. Dense vegetation provides more fuel supply, so the fire intensity is also high. Rogers et al. concluded that the continental difference in boreal fires between Eurasia and North America can be attributed to the differences in species-level traits between these two northern continents. According to the functional diversity of boreal Eurasia, three vegetation zones with different dominant tree species have been identified: northwest Eurasia (most of the "dark taiga" in the continent), northeast Eurasia (deciduous larch), and south Eurasia (undergrowth grasses) [59]. In these zones, fire regimes are different. In northwest Eurasia, higher wildfire frequency due to more avoider forests has been observed than in the other two Eurasian regions. In northeast Eurasia, deciduous larch is dominated due to a harsher continental climate which is less likely to cause wildfires than relatively flammable vegetation such as herbs [60, 61]. The pollen data from sediment core PG1351 in the Lake El'gygytgyn show that herbs are dominant during glacial periods while an expansion of tree and shrubs during interglacial periods [62]. Chlachula reconstructed the vegetation history during the Pleistocene and the Holocene in east Siberia according to the sediment records of Lake Baikal [63], which showed Pinus and Artemisia were the main species during glacial periods. Compared with the glacial periods, the interglacial climate was suitable for the vegetation growth, thus with more abundant vegetation types and the total amount of combustible vegetation. However, our records of wildfires during the glacial periods showed a higher frequency of wildfires. On orbital, the continuous existence of soot and char observed in core LV76-18 indicates a persistent biomass burning and supply of available fuel load from Siberia. Therefore, we argue that the vegetation structure and composition are not a crucial factor in controlling the frequency of region and/or hemisphere-wide high-intensity wildfires.

Available fuel load, however, has crucial effects on the development of wildfire. In particular, the expansion of Northern Hemisphere ice sheets during glacial periods through the Quaternary may change the terrestrial landscape and vegetation, thus changing the amount of fuel available for fire. According to the synthesis of the experimental data and numerical simulation results, Batchelor et al. found that ice-marginal positions and ice-sheet extent between glacial cycles varied greatly [38]. Particularly, a larger ice-sheet extent occurred during MIS6 in northeast Siberia than in the LGM, corresponding to the decrease in fuel supply and downward trend of high-intensity fire frequency during MIS6, as shown by the mass accumulation rate of soot in core LV76-18. In contrast, the ice-sheet extent in northeast Siberia was less during other glacial periods (MIS2, 4, 8) [38], so its impact on vegetation and fuel load was minimal. We argue that the contrasting pattern of high-intensity wildfire frequency between MIS6 and other glacial periods is ascribed to the different North Hemisphere ice sheet configurations at these times.

Spectral analysis shows that soot records have significant a precession cycle of 23 ka in the 90% confidence interval, indicating that the fundamental driving force of fire activity in Siberia is climate change caused by variations in orbital precession (Figure 8). Orbital-scale variations in low-latitude insolation are primarily controlled by precession [64, 65], which was directly linked to changes in the intensity of the EASM driven by variations in insolation [53]. During weak EASM, less moisture is transported to Asian inland,

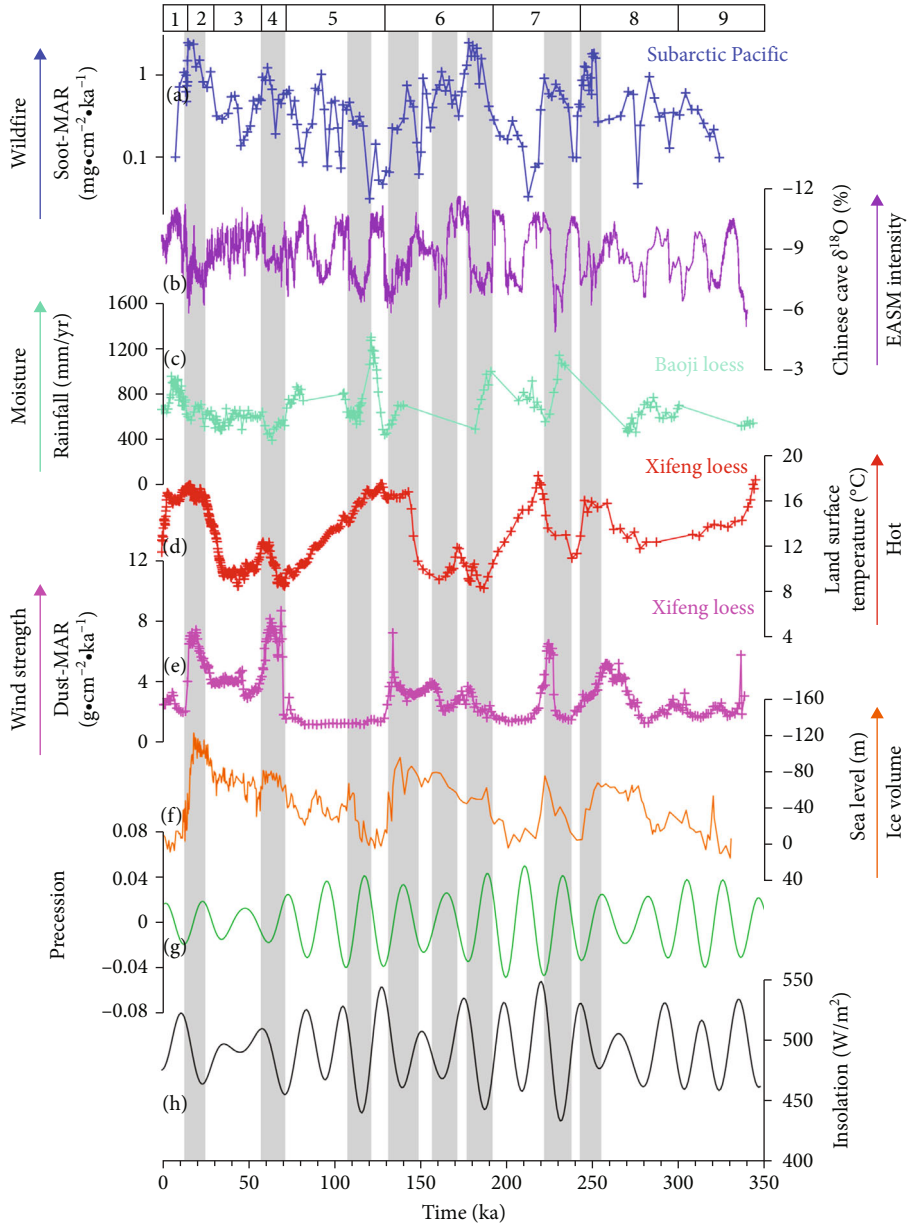


FIGURE 8: LV76-18 wildfire records compared with the climatic and orbital parameter factors during the past 320 ka. (a) LV76-18 soot-MARs (this study); (b) Chinese stalagmites $\delta^{18}$O [53]; (c) rainfall record from Baoji loess [54]; (d) land surface temperature (LST) from Xifeng Loess [56]; (e) Xifeng dust-MARs [40]; (f) sea level [57]; (g) precession [58]; (h) 65°N insolation in June [58]; the grey-shaded bars represent the correspondence between peaks of soot-MARs and other factors.

thus less precipitation and more dryness. An insufficient supply of moisture in the root zone caused by the decrease in monsoon precipitation may limit transpiration and canopy humidity in the subsequent dry season [66]. Global cooling and the expansion of the Northern Hemisphere ice sheet are also considered to play crucial roles in controlling the drought in the Asian inland [3]. On the other hand, the intensification and equatorward displacement of the northern westerly due to larger temperature gradient between the tropic and the high latitude and ice volume during glacial periods favor the production and transport of both soot and dust. All these climatic backgrounds have created favorable conditions for biomass burning and subsequent transportation of soot.

The correlation phase analysis further confirmed the effects of precession on reasoning. Figure 9 shows a close relationship between soot records and the EASM, EAWM, and ice volume. In the Milankovitch periodic frequency bands of 23 ka and 41 ka, the EAM and global ice volume all precede the soot records. In particular, in the precession band of 23 ka, the correlation between these three indicators and soot is high and in phase. Although the relationship between wildfire and climate factors is complex and nonlinear, there is no doubt that these arguments undoubtedly

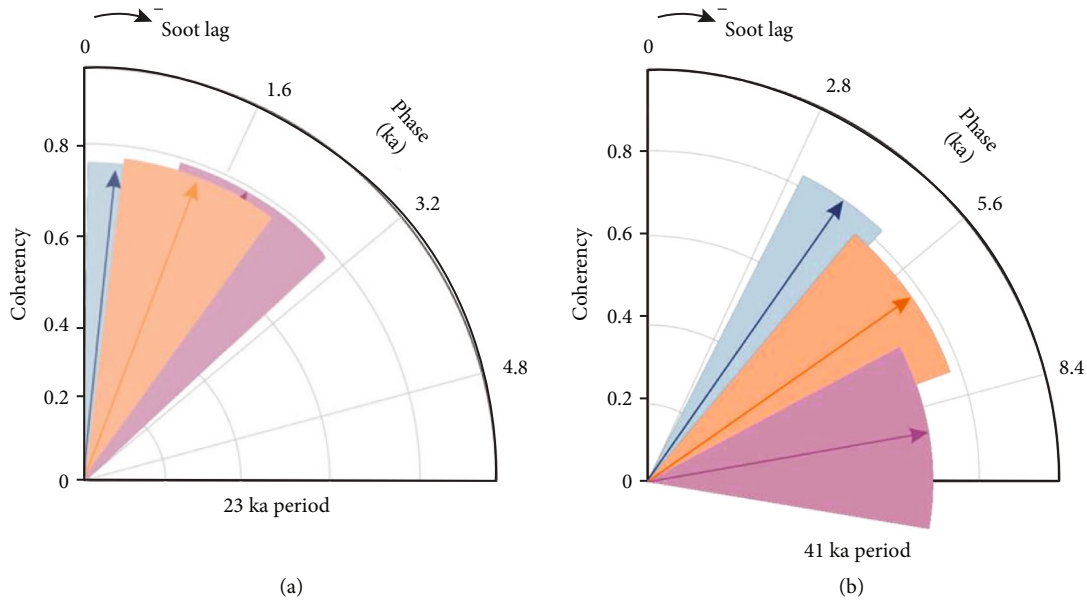


FIGURE 9: Coherency phase of soot against the Asian summer monsoon [53] (light pink arrow), East Asian winter monsoon [3] (light blue arrow), and ice volume [67] (orange arrow) in the 23 $ka^{-1}$ and 41 $ka^{-1}$ frequency bands. The arrow length represents coherency, and the shaded areas are the phase error at the 95% confidence level. Soot lags behind the ASM, ASWM, and ice volume.

confirm the above-mentioned relationship, that is, high-intensity wildfires are more likely to occur in dry periods, which is closely related to the precession of the Earth's orbital.

## 5. Conclusions

In summary, BC has been proved to be an effective proxy of wildfire reconstruction [9, 12, 22]. Particularly for the soot, because of its small particle size and long transport range, it can indicate regional or hemispheric fires to some extent and it is more suitable for the reconstruction of wildfire records in open sea areas. On this basis, we investigated the soot records of the deep-sea sediment core LV76-18 and the wildfire activity in Eurasia over the past 320 ka. The main conclusions are as follows:

(1) Over the past 320 ka, our wildfire reconstruction showed clear glacial-interglacial cycles and high-intensity fire occurred during the glacial periods. In general, the increase in high-intensity wildfires is closely related to the increase in drought, which is due to the decrease in precipitation

(2) The record of wildfire shows a remarkable 23 ka precession cycle, indicating that the climate condition controlled by changes in Earth's orbital precession is the main driver of wildfire

(3) There is a close interaction between wildfire and climate. We argue that the soluble micronutrients from wildfires, such as Fe and P, have the potential to improve nutrient utilization efficiency, in the subarctic Pacific. We suggest that the potential feedback of wildfires to the climate system needs to be further investigated

## Data Availability

Data of this study can be available for all interested researchers upon request (zoujianjun@fio.org.cn; bingchen@sdu.edu.cn).

## Additional Points

*Highlights*. A 320 ka long wildfire record with black carbon was reported from a sediment core taken from the subarctic North Pacific. Higher-frequency occurrence of wildfire took place during glacial periods. Climate and climate-modulated changes in vegetation cover control the Eurasia wildfire over glacial-interglacial cycles. There is a tight coupling between Eurasia wildfire and nutrient utilization efficiency in the subarctic North Pacific.

## Conflicts of Interest

The authors declare that they have no conflict of interest.

## Acknowledgments

The funding for this research was supported by the Marine S&T Fund of Shandong Province for Pilot National Laboratory for Marine Science and Technology (Qingdao) (Grant No. 2022QNLM050203), the Basic Scientific Fund for National Public Research Institutes of China (No. GY0222G01), and the Taishan Scholar Foundation of Shandong Province (Grant No. TSPD20181216).

## Supplementary Materials

Example of thermal spectrogram measured by the Sunset carbon analyzer. *(Supplementary Materials)*

## References


[1] D. Bowman, J. K. Balch, P. Artaxo et al., "Fire in the earth system," *Science*, vol. 324, no. 5926, pp. 481–484, 2009.

[2] S. Archibald, C. E. Lehmann, C. M. Belcher et al., "Biological and geophysical feedbacks with fire in the earth system," *Environmental Research Letters*, vol. 13, no. 3, p. 18, 2018.

[3] Y. M. Han, Z. An, J. R. Marlon et al., "Asian inland wildfires driven by glacial-interglacial climate change," *Proceedings of the National Academy of Sciences of the United States of America*, vol. 117, no. 10, pp. 5184–5189, 2020.

[4] A. L. Daniau, S. P. Harrison, and P. J. Bartlein, "Fire regimes during the last glacial," *Quaternary Science Reviews*, vol. 29, no. 21-22, pp. 2918–2930, 2010.

[5] T. Kitzberger, P. M. Brown, E. K. Heyerdahl, T. W. Swetnam, and T. T. Veblen, "Contingent Pacific-Atlantic Ocean influence on multicentury wildfire synchrony over western North America," *Proceedings of the National Academy of Sciences of the United States of America*, vol. 104, no. 2, pp. 543–548, 2007.

[6] L. Wu, L. Li, H. Zhou, X. Wang, and G. Zhang, "Holocene fire in relation to environmental change and human activity reconstructed from sedimentary charcoal of Chaohu Lake, East China," *Quaternary International*, vol. 507, pp. 62–73, 2019.

[7] S. van der Kaars, X. Wang, P. Kershaw, F. Guichard, and D. A. Setiabudi, "A Late Quaternary palaeoecological record from the Banda Sea, Indonesia: patterns of vegetation, climate and biomass burning in Indonesia and northern Australia," *Palaeogeography Palaeoclimatology Palaeoecology*, vol. 155, no. 1-2, pp. 135–153, 2000.

[8] M. I. Bird and J. A. Cali, "A million-year record of fire in sub-Saharan Africa," *Nature*, vol. 394, no. 6695, pp. 767–769, 1998.

[9] M. Conedera, W. Tinner, C. Neff, M. Meurer, A. F. Dickens, and P. Krebs, "Reconstructing past fire regimes: methods, applications, and relevance to fire management and conservation," *Quaternary Science Reviews*, vol. 28, no. 5-6, pp. 555–576, 2009.

[10] Z. H. Tan, Y. Han, J. Cao, C. Chang Huang, and Z. An, "Holocene wildfire history and human activity from high-resolution charcoal and elemental black carbon records in the Guanzhong Basin of the Loess Plateau, China," *Quaternary Science Reviews*, vol. 109, pp. 76–87, 2015.

[11] Z. H. Tan, C. C. Huang, J. Pang, and Q. Zhou, "Holocene wildfires related to climate and land-use change over the Weihe River Basin, China," *Quaternary International*, vol. 234, no. 1-2, pp. 167–173, 2011.

[12] X. Wang, P. A. Peng, and Z. L. Ding, "Black carbon records in Chinese Loess Plateau over the last two glacial cycles and implications for paleofires," *Palaeogeography Palaeoclimatology Palaeoecology*, vol. 223, no. 1-2, pp. 9–19, 2005.

[13] Y. M. Han, D. M. Peteet, R. Arimoto et al., "Climate and fuel controls on North American paleofires: smoldering to flaming in the Late-glacial-Holocene transition," *Scientific Reports*, vol. 6, p. 8, 2016.

[14] A. Kappenberg, E. Lehndorff, N. Pickarski, T. Litt, and W. Amelung, "Solar controls of fire events during the past 600,000 years," *Quaternary Science Reviews*, vol. 208, pp. 97–104, 2019.

[15] S. Archibald, D. P. Roy, B. W. van Wilgen, and R. J. Scholes, "What limits fire? An examination of drivers of burnt area in southern Africa," *Global Change Biology*, vol. 15, no. 3, pp. 613–630, 2009.

[16] D. M. Nelson, D. Verschuren, M. A. Urban, and F. S. Hu, "Long-term variability and rainfall control of savanna fire regimes in equatorial East Africa," *Global Change Biology*, vol. 18, no. 10, pp. 3160–3170, 2012.

[17] R. Xu, P. Yu, M. J. Abramson et al., "Wildfires, global climate change, and human health," *The New England Journal of Medicine*, vol. 383, no. 22, pp. 2173–2181, 2020.

[18] Y. M. Han, J. R. Marlon, J. J. Cao, Z. D. Jin, and Z. S. An, "Holocene linkages between char, soot, biomass burning and climate from Lake Daihai, China," *Global Biogeochemical Cycles*, vol. 26, no. 4, p. 9, 2012.

[19] M. Wolf, E. Lehndorff, M. Mrowald et al., "Black carbon: fire fingerprints in Pleistocene loess-palaeosol archives in Germany," *Organic Geochemistry*, vol. 70, pp. 44–52, 2014.

[20] B. Zhou, C. Shen, W. Sun et al., "Elemental carbon record of paleofire history on the Chinese Loess Plateau during the last 420 ka and its response to environmental and climate changes," *Palaeogeography Palaeoclimatology Palaeoecology*, vol. 252, no. 3-4, pp. 617–625, 2007.

[21] S. D. Mooney, S. P. Harrison, P. J. Bartlein et al., "Late Quaternary fire regimes of Australasia," *Quaternary Science Reviews*, vol. 30, no. 1-2, pp. 28–46, 2011.

[22] Y. M. Han, Z. S. An, and J. J. Cao, "The Anthropocene–a potential stratigraphic definition based on black carbon, char, and soot records," vol. 1, pp. 171–178, 2018.

[23] Y. Hao, Y. Han, Z. An, and G. S. Burr, "Climatic control of orbital time-scale wildfire occurrences since the late MIS 3 at Qinghai Lake, monsoon marginal zone," *Quaternary International*, vol. 550, pp. 20–26, 2020.

[24] Y. N. Han, J. Cao, Z. An et al., "Evaluation of the thermal/optical reflectance method for quantification of elemental carbon in sediments," *Chemosphere*, vol. 69, no. 4, pp. 526–533, 2007.

[25] Y. Fang, Y. Chen, C. Tian et al., "Flux and budget of BC in the continental shelf seas adjacent to Chinese high BC emission source regions," *Global Biogeochemical Cycles*, vol. 29, no. 7, pp. 957–972, 2015.

[26] Y. M. Han, J. J. Cao, B. Z. Yan et al., "Comparison of elemental carbon in lake sediments measured by three different methods and 150-year pollution history in eastern China," *Environmental Science & Technology*, vol. 45, no. 12, pp. 5287–5293, 2011.

[27] Y. Fang, Y. Chen, T. Lin et al., "Spatiotemporal trends of elemental carbon and char/soot ratios in five sediment cores from eastern China marginal seas: indicators of anthropogenic activities and transport patterns," *Environmental Science & Technology*, vol. 52, no. 17, pp. 9704–9712, 2018.

[28] A. I. Coppola, D. B. Wiedemeier, V. Galy et al., "Publisher correction: global-scale evidence for the refractory nature of riverine black carbon," *Nature Geoscience*, vol. 11, no. 12, pp. 966–966, 2018.

[29] Y. Q. Wang, "MeteoInfo: GIS software for meteorological data visualization and analysis," *Meteorological Applications*, vol. 21, no. 2, pp. 360–368, 2014.

[30] J. S. Nie, A. Pullen, C. N. Garzione, W. Peng, and Z. Wang, "Pre-Quaternary decoupling between Asian aridification and

high dust accumulation rates," *Science Advances*, vol. 4, no. 2, p. 8, 2018.

[31] L. E. Lisiecki and M. E. Raymo, "A Pliocene-Pleistocene stack of 57 globally distributed benthic δ18O records," *Paleoceanography*, vol. 20, no. 1, p. 17, 2005.

[32] S. A. Gorbarenko, E. A. Yanchenko, O.'. Y. Psheneva et al., "Orbital and millennial-scale environmental and hydrological changes of the central Okhotsk Sea over the last 136 kyr inferred from micropaleontological (radiolarian and benthic foraminifera), geochemical and lithological proxies and the mechanisms responsible for them," *Quaternary Science Reviews*, vol. 247, p. 106569, 2020.

[33] K. Hammes, M. W. I. Schmidt, R. J. Smernik et al., "Comparison of quantification methods to measure fire-derived (black/elemental) carbon in soils and sediments using reference materials from soil, water, sediment and the atmosphere," *Global Biogeochemical Cycles*, vol. 21, no. 3, p. 18, 2007.

[34] Z. Y. Cong, S. Kang, S. Gao, Y. Zhang, Q. Li, and K. Kawamura, "Historical trends of atmospheric black carbon on Tibetan Plateau as reconstructed from a 150-year lake sediment record," *Environmental Science & Technology*, vol. 47, no. 6, pp. 2579–2586, 2013.

[35] S. Tiwari, L. Kun, and B. Chen, "Spatial variability of sedimentary carbon in South Yellow Sea, China: impact of anthropogenic emission and long-range transportation," *Environmental Science and Pollution Research*, vol. 27, no. 19, pp. 23812–23823, 2020.

[36] W. X. Xu, F. Wang, J. Li et al., "Historical variation in black carbon deposition and sources to northern China sediments," *Chemosphere*, vol. 172, pp. 242–248, 2017.

[37] C. Gao, Q. Lin, S. Zhang, J. He, X. Lu, and G. Wang, "Historical trends of atmospheric black carbon on Sanjiang Plain as reconstructed from a 150-year peat record," *Scientific Reports*, vol. 4, no. 1, 2015.

[38] C. L. Batchelor, M. Margold, M. Krapp et al., "The configuration of Northern Hemisphere ice sheets through the Quaternary," *Nature Communications*, vol. 10, no. 1, p. 3713, 2019.

[39] S. A. Hovan, D. K. Rea, and N. G. Pisias, "Late Pleistocene continental climate and oceanic variability recorded in northwest Pacific sediments," *Paleoceanography*, vol. 6, no. 3, pp. 349–370, 1991.

[40] Z. T. Guo, S. Z. Peng, Q. Z. Hao, P. E. Biscaye, and T. S. Liu, "Origin of the Miocene-Pliocene red-earth formation at Xifeng in northern China and implications for paleoenvironments," *Palaeogeography Palaeoclimatology Palaeoecology*, vol. 170, no. 1-2, pp. 11–26, 2001.

[41] E. Maier, B. Chapligin, A. Abelmann et al., "Combined oxygen and silicon isotope analysis of diatom silica from a deglacial subarctic Pacific record," *Journal of Quaternary Science*, vol. 28, no. 6, pp. 571–581, 2013.

[42] D. Lüthi, M. Le Floch, B. Bereiter et al., "High-resolution carbon dioxide concentration record 650,000-800,000 years before present," *Nature*, vol. 453, no. 7193, pp. 379–382, 2008.

[43] A. L. Daniau, M. F. Sánchez Goñi, P. Martinez et al., "Orbital-scale climate forcing of grassland burning in southern Africa," *Proceedings of the National Academy of Sciences of the United States of America*, vol. 110, no. 13, pp. 5069–5073, 2013.

[44] M. J. Power, J. Marlon, N. Ortiz et al., "Changes in fire regimes since the last glacial maximum: an assessment based on a global synthesis and analysis of charcoal data," *Climate Dynamics*, vol. 30, no. 7-8, pp. 887–907, 2008.

[45] O. Marchal, R. François, T. F. Stocker, and F. Joos, "Ocean thermohaline circulation and sedimentary231Pa/230Th ratio," *Paleoceanography*, vol. 15, no. 6, pp. 625–641, 2000.

[46] E. Dietze, K. Mangelsdorf, A. Andreev et al., "Relationships between low-temperature fires, climate and vegetation during three late glacials and interglacials of the last 430 kyr in northeastern Siberia reconstructed from monosaccharide anhydrides in Lake El'gygytgyn sediments," *Climate of the Past*, vol. 16, no. 2, pp. 799–818, 2020.

[47] V. Ramanathan and G. Carmichael, "Global and regional climate changes due to black carbon," *Nature Geoscience*, vol. 1, no. 4, pp. 221–227, 2008.

[48] J. T. Randerson, H. Liu, M. G. Flanner et al., "The impact of boreal forest fire on climate warming," *Science*, vol. 314, no. 5802, pp. 1130–1132, 2006.

[49] A. L. Daniau, P. J. Bartlein, S. P. Harrison et al., "Predictability of biomass burning in response to climate changes," *Global Biogeochemical Cycles*, vol. 26, no. 4, p. 12, 2012.

[50] A. Feurdean, G. Florescu, I. Tanţău et al., "Recent fire regime in the southern boreal forests of western Siberia is unprecedented in the last five millennia," *Quaternary Science Reviews*, vol. 244, p. 106495, 2020.

[51] O. Pechony and D. T. Shindell, "Driving forces of global wildfires over the past millennium and the forthcoming century," *Proceedings of the National Academy of Sciences of the United States of America*, vol. 107, no. 45, pp. 19167–19170, 2010.

[52] Z. Y. Gu, D. Lal, T. S. Liu et al., "Five million year 10Be record in Chinese loess and red-clay: climate and weathering relationships," *Earth and Planetary Science Letters*, vol. 144, no. 1-2, pp. 273–287, 1996.

[53] H. Cheng, R. L. Edwards, A. Sinha et al., "Correction: Corrigendum: The Asian monsoon over the past 640,000 years and ice age terminations," *Nature*, vol. 541, no. 7635, pp. 122–122, 2017.

[54] J. W. Beck, W. Zhou, C. Li et al., "A 550,000-year record of east Asian monsoon rainfall from10Be in loess," *Science*, vol. 360, no. 6391, pp. 877–881, 2018.

[55] Y. J. Wang, H. Cheng, R. L. Edwards et al., "A high-resolution absolute-dated Late Pleistocene monsoon record from Hulu Cave, China," *Science*, vol. 294, no. 5550, pp. 2345–2348, 2001.

[56] H. X. Lu, W. Liu, H. Yang et al., "800-kyr land temperature variations modulated by vegetation changes on Chinese Loess Plateau," *Nature Communications*, vol. 10, no. 1, p. ???, 2019.

[57] J. Jouzel, V. Masson-Delmotte, O. Cattani et al., "Orbital and millennial Antarctic climate variability over the past 800,000 years," *Science*, vol. 317, no. 5839, pp. 793–796, 2007.

[58] A. L. Berger, "Long-term variations of caloric insolation resulting from the Earth's orbital elements," *Quaternary Research*, vol. 9, no. 2, pp. 139–167, 1978.

[59] B. M. Rogers, A. J. Soja, M. L. Goulden, and J. T. Randerson, "Influence of tree species on continental differences in boreal fires and climate feedbacks," *Nature Geoscience*, vol. 8, no. 3, pp. 228–234, 2015.

[60] V. V. Furyaev, E. A. Vaganov, N. M. Tchebakova, and E. N. Valendik, "Effects of fire and climate on successions and structural changes in the Siberian boreal forest," *Eurasian Journal of Forest Research*, vol. 2, pp. 1–15, 2001.

[61] D. J. McRae, S. G. Conard, G. A. Ivanova et al., "Variability of fire behavior, fire effects, and emissions in scotch pine forests of central Siberia," *Mitigation and Adaptation Strategies for Global Change*, vol. 11, no. 1, pp. 45–74, 2006.

[62] N. R. Nowaczyk, P. Minyuk, M. Melles et al., "Magnetostratigraphic results from impact crater Lake El'gygytgyn, northeastern Siberia: a 300 kyr long high-resolution terrestrial palaeoclimatic record from the Arctic," *Geophysical Journal International*, vol. 150, no. 1, pp. 109–126, 2002.

[63] J. Chlachula, "Pleistocene climate change, natural environments and palaeolithic occupation of the Angara-Baikal area, east central Siberia," *Quaternary International*, vol. 80-81, pp. 69–92, 2001.

[64] A. C. Clement, A. Hall, and A. J. Broccoli, "The importance of precessional signals in the tropical climate," *Climate Dynamics*, vol. 22, no. 4, pp. 327–341, 2004.

[65] J. Imbrie, A. Berger, E. A. Boyle et al., "On the structure and origin of major glaciation cycles 2. The 100,000-year cycle," *Paleoceanography*, vol. 8, no. 6, pp. 699–735, 1993.

[66] D. L. Ning, E. Zhang, J. Shulmeister, J. Chang, W. Sun, and Z. Ni, "Combining and competing effects between precipitation and temperature on Holocene fire regime evolution inferred from a sedimentary black carbon record in southwestern China," *Quaternary Research*, vol. 93, no. 1, pp. 243–254, 2020.

[67] M. E. Raymo, L. E. Lisiecki, and K. H. Nisancioglu, "Plio-pleistocene ice volume, Antarctic climate, and the global δ18O record," *Science*, vol. 313, no. 5786, pp. 492–495, 2006.